Hindawi
Journal of Nanomaterials
Volume 2020, Article ID 7680508, 11 pages
https://doi.org/10.1155/2020/7680508

Research Article

Ammonia Gas Sensing Behavior of Hybridization between Reduced Graphene Oxide and Gold Nanoparticles

Huynh Tran My Hoa,[1] Kang Jea Lee,[1] Hoai Phuong Pham,[1] Tuan Anh Doan,[1] Hoang Hung Nguyen,[2] Tran Quang Nguyen,[2] Quang Trung Tran,[2] and Tran Viet Cuong[1]

[1]*VKTECH Research Center, Nguyen Tat Thanh University, 298-300A Nguyen Tat Thanh Street, Ward 13, District 4, Ho Chi Minh City, Vietnam*
[2]*Department of Solid State Physics, Faculty of Physics, University of Sciences, Vietnam National University Ho Chi Minh City (VNU-HCM), 227 Nguyen Van Cu, District 5, Ho Chi Minh City, Vietnam*

Correspondence should be addressed to Tran Viet Cuong; tvcuong@ntt.edu.vn

Received 19 February 2020; Revised 28 July 2020; Accepted 13 August 2020; Published 28 August 2020

Academic Editor: Kishore Sridharan

Stack and composite are the two ways of hybridization between gold nanoparticles (AuNPs) and reduced graphene oxide (rGO) which have been fabricated and tested the ability to detect NH_3 gas at room temperature. The device based on the rGO-AuNP composite structure exhibited the highest response and the fastest response and recovery time compared to stack and bare rGO. The red shift of a resonant peak in the absorption spectra and the negative shift in the binding energy of $4f_{5/2}$ peak indicated that the remarkable NH_3 gas-sensing properties of this composite are mainly attributed to a chemical bonding formed between AuNPs and rGO at the defective sites. This type of interaction facilitates the electron transfer from the defect states to the AuNP surface wherein it easily reacts with the oxygen molecules in the atmosphere to create oxygen absorbents. Consequently, NH_3 not only reacts with sp^3-hybridized atoms but also reacts primarily with oxygen absorbents on the surface of AuNPs, resulting in a better sensing behavior of composite samples.

1. Introduction

In the past few years, reduced graphene oxide (rGO) has emerged as an alternative to graphene because it is possible to tailor and create "new functionalities" of graphene through defects and oxygen-containing functional groups [1]. Particularly for gas sensor applications, oxygen-related groups on the graphene surface are favorable for the adsorption of analytes, thus enabling detecting at lower concentrations of gases. Meanwhile, defects act as active sites in forming nanocomposites with noble metals by the process of hybridization. It is believed that the sensing performances are expected to dramatically enhance via functionalizing the surface of rGO with catalytic metals (Pt, Pd, Ag, Cu, and Au), owing to the synergistic effect of the hybrid configuration [2, 3]. For example, using rGO and $HAuCl_4$ precursors, Zhang and coworkers prepared rGO/Au composite via hydrothermal treatment (at 180°C for 12 hours) and fabricated gas sensors for NO_2 detection at 50°C. Meanwhile, Sivalingam and Balasubramanian use the coreduction method of these precursors (at 80°C for 5 minutes) to synthesize rGO/Au film which was applied to NH_3 sensing at RT [4, 5]. Choi et al. synthesize rGO and then deposit the Pd layer on the rGO surface by a sputtering process and thermal annealing; a NO_2 gas sensor at RT was made from this Pd-rGO hybrid [6]. From these reports, it can be seen that the mechanism and performance of the sensor depend strongly on the metal used and the synthesis method. Indeed, it comes from the fact that the type of interactions between rGO and noble metals vary from weak van der Waals to strong covalent bonding which makes a clear difference in the sensing activities of rGO-metal hybrid devices. Several theoretical and experimental studies on the interaction between graphene and noble metals have been performed, but similar studies for the rGO-metal hybrid

are still limited in the literature [7–9]. In this study, we focus on fabricating two types of combinations of rGO and AuNPs such as layer-by-layer (stack) and composite to clarify the correlation between AuNPs and rGO. Hopefully, this study will help elucidate the relationship between the sensor activities of rGO-AuNP hybrid toward NH_3 gas and the interaction of rGO and AuNPs.

2. Experimental Method

2.1. Synthesis of Aqueous GO Dispersion. We synthesized aqueous graphene oxide (GO) dispersion from graphite powder using a modified Hummers method. For a detailed description, 0.2 g of graphite flake, 0.1 g of $NaNO_3$, and 0.8 g of $KMnO_4$ were added to 16 ml of H_2SO_4 under stirring and cooling at 0°C in a flask for 2 hours. Consequently, 32 ml of deionized (DI) water was slowly drop-casted after stirring this suspension at room temperature for more than 1 hour. Finally, 5 ml of 30% H_2O_2 was added to the diluted suspension and it turned yellow-brownish, indicating the formation of GO. The 5% HCl solution used to dissolve the residual metals and the resulting GO suspension (pH ~1) was separated using centrifugation at 5,000 rpm for 5 min. The GO was further washed with DI water under the same centrifugal conditions until pH equals to 7. The synthesized GO was then dispersed in DI water to form a 2.5 mg/ml GO aqueous solution.

2.2. Preparation of rGO/AuNP Stack. To synthesize AuNPs, 1.25 ml of $HAuCl_4$ (1 mg/ml) and 0.25 ml of $C_6H_5Na_3O_7$ (10 mg/ml) were sequentially added to 5 ml of DI water and vigorously stirred for 15 min. Next, 0.5 ml of $NaBH_4$ (0.4 mg/ml) was slowly added dropwise to reduce gold ions in the precursor solution and keep stirring for 30 min. The gold nanoparticles were isolated using centrifugation at 12,000 rpm for 5 min and were redispersed in DI water. To obtain rGO/AuNP stack (sample A), 1.0 ml of GO aqueous solution (2.5 mg/ml) and the AuNP solution (0.5 mg/ml) were sequentially sprayed on a preheated substrate as illustrated in Figure 1. Finally, N_2H_4 vapor at an elevated temperature of 80°C and thermal annealing 350°C were combined to reduce GO to rGO.

2.3. Preparation of rGO-AuNP Composite. To produce rGO-AuNP composite (sample B), 1.0 ml of GO aqueous suspension (2.5 mg/ml) and 1.25 ml of $HAuCl_4$ (1.0 mg/ml) were added in 5 ml of water. The resultant suspension was stabilized for 30 min to promote the interaction of gold ions with GO surface. Then, 0.25 ml of $C_6H_5Na_3O_7$ (10 mg/ml) was added at an elevated temperature of 80°C. The reaction was kept at this condition for 1 hour. To remove the free AuNPs in solution, the centrifugation was performed at 7,000 rpm for 5 min. The resultant GO-AuNP solution and 0.5 ml of $NaBH_4$ (0.4 mg/ml) were mixed in 5 ml of DI water and stirred for 10 min to convert GO-AuNPs into rGO-AuNPs. Finally, the as-prepared rGO-AuNP solution was sprayed on a heated substrate at 350°C to form rGO-AuNP composite (Figure 1).

2.4. Material Characterizations and Gas Testing. Two ways of combining between rGO sheets and AuNPs such as stack and composite have been carried out. First, individual components such as AuNPs and rGO constituting the hybrids were analyzed individually using the following measurements: transmission electron microscopy (TEM) and the X-ray diffraction (XRD) measurements were applied to define the size and crystalline nature of the AuNPs; Raman and X-ray photoelectron spectroscopy (XPS) are employed to investigate rGO. Second, the surface morphology of prepared rGO-AuNP hybrids was characterized using atomic force microscopy (AFM), scanning electron microscopy (SEM), and XPS. The typical current-voltage measurement and UV-Vis spectroscopy were performed for electrical and optical characterization.

The process for fabricating two sensor devices based on rGO/AuNP stack and rGO-AuNP composite is illustrated in Figure 1(a). Their response toward NH_3 gas at room temperature was compared under identical testing conditions. A diagram of a gas sensor measurement system is shown in Figure 1(b). The measuring chamber is made up of volume 500 cm^3 in the presence of air atmosphere and NH_3 gas at room temperature (300 K). The gas flow rate was controlled with a mass flow controller. The change of the sensor resistance due to NH_3 adsorption was monitored, analyzed, and stored by a computer with a data acquisition board and LabView software. Based on this design, the NH_3 gas is diluted into an inert carrier gas to produce different concentrations of test gas. Therefore, the diluted concentration is defined from the volumetric flow rate of the test gas and the carrier gas as well as the concentration of the cylinder of test gas. The response of the sensor to NH_3 is defined as the ratio of change in the resistance of the sample on exposure to ammonia to the resistance in the air.

$$\Delta R\,(\%) = 100\% \times \frac{R_g - R_a}{R_a}, \tag{1}$$

where R_g and R_a are sensing material resistance, measured in NH_3 and air atmosphere, respectively.

3. Results and Discussion

The properties of the individual materials that make up the composition are investigated in detail in Figure 2. Firstly, as-synthesized AuNP size is determined using a transmission electron microscopy as shown in Figure 2(a). A TEM image of AuNPs displays an average size of 10–20 nm with an indefinite shape. X-ray diffraction measurement is applied to define the crystalline nature of the AuNPs. Figure 2(b) shows the diffraction pattern of AuNPs with three main peaks appearing at 2θ values of 38.2°, 44.5°, and 65.1° which are assigned to (111), (200), and (220) crystallographic planes AuNPs. Secondly, Raman (Figure 2(c)) and XPS (Figure 2(d)) measurements are employed to qualitatively characterize graphene-related materials. Two fundamental peaks at 1320 cm^{-1} and 1590 cm^{-1}, which correspond to the disorder induced by the D and G bands of carbon atoms,

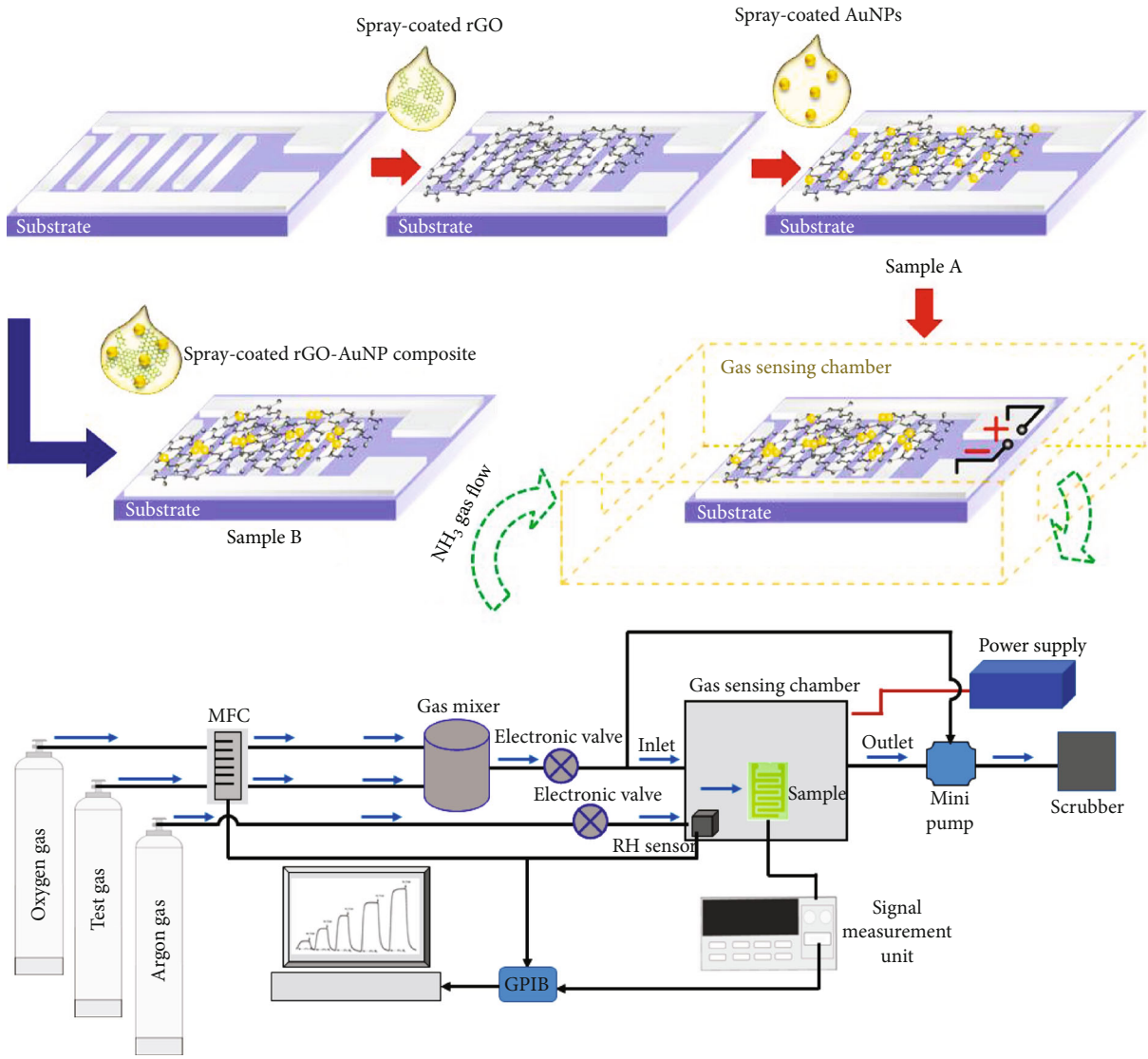

Figure 1: Schematic illustration of the process to produce sample A (rGO/AuNP stack) and sample B (rGO-AuNP composite) and the diagram of the gas-sensing measurement system.

were observed in the Raman spectra of GO and rGO. The G band arises from the E_{2g} emission of the zone-center optical phonons of C sp^2 atoms (usually observed at 1575 cm^{-1}), and the D band arises from the breathing mode of k-point photons of A_{1g} symmetry mode activated by the presence of disorder on graphene sheets (at 1350 cm^{-1}). Indeed, it is clear to see that D peak intensity in the GO sample was higher than that of rGO and graphite samples. This implies that the number of disorders caused by oxygen-containing groups decreases during the transformation process from amorphous (GO) to nanocrystalline graphite (rGO). To validate this explanation, the C1s XPS core-level spectrum of rGO is displayed in Figure 2(d). As compared to the C1s spectra of GO as shown in the inset, the peak intensities of oxygen-containing groups (C=O, C-O, and O=C-OH) decrease dramatically and aromatic lattice peak intensity (C=C, C-C) increases in rGO. It demonstrates the effective removal of oxygen-containing functional groups from GO during the reduction process.

Figure 3 represents SEM and AFM images of rGO/AuNP stack and rGO-AuNP composite samples. Samples A and B have distinct surface morphology where Au nanoparticles show the difference in size and arrangement manner on the rGO surface (Figures 3(a) and 3(c)). The AFM image of sample A, Figure 3(b), indicates that AuNPs randomly distribute on the whole rGO surface, while AuNPs in sample B arrange as cluster forms at some specific sites as shown in Figure 3(d). The aggregation of AuNPs in sample B is observed in the inset SEM image of Figure 3(c). It results from the fact that Au ions in precursor solution often tend to bind with oxygen functional groups, which agglomerate at defect sites on the surface and the edges of GO sheets, via dangling bonds to form AuNP clusters during the reduction step. It is reported that there are differences of metal nanoparticles that interact with rGO sheets at different sites, i.e., the defective sites are more favorable compared to defect-free areas in the attachment of metal nanoparticles [1, 10]. Considering the size of AuNPs, the AFM images reveal that sample A contains

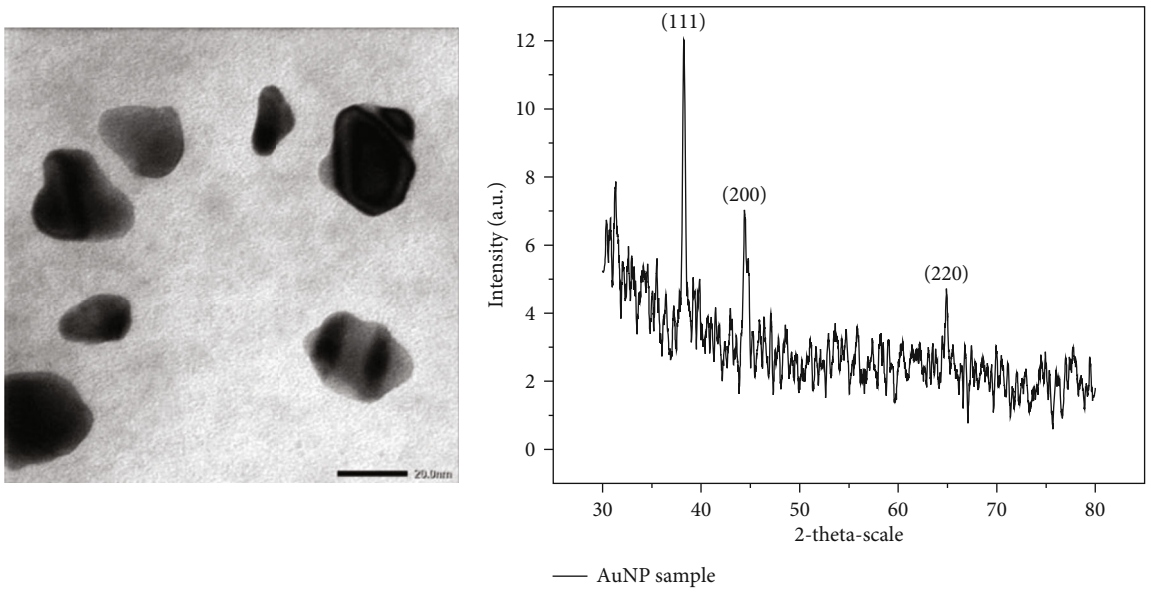

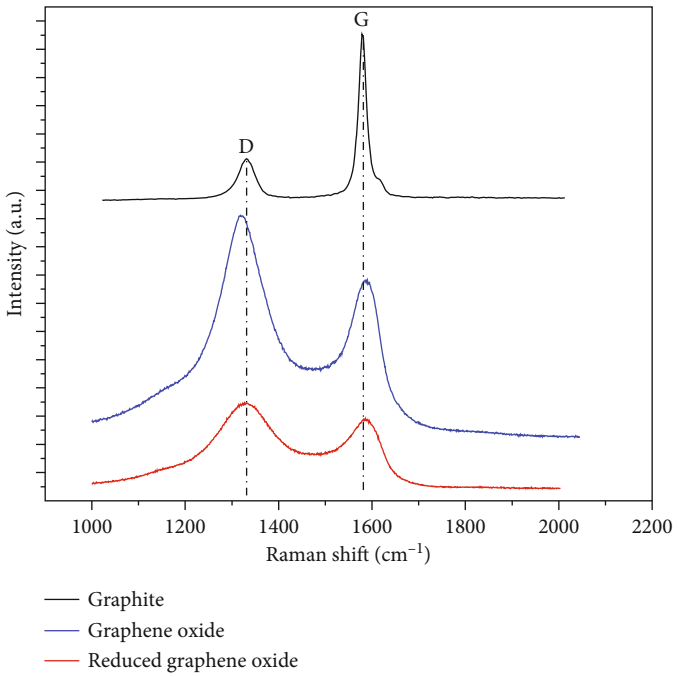

Figure 2: Continued.

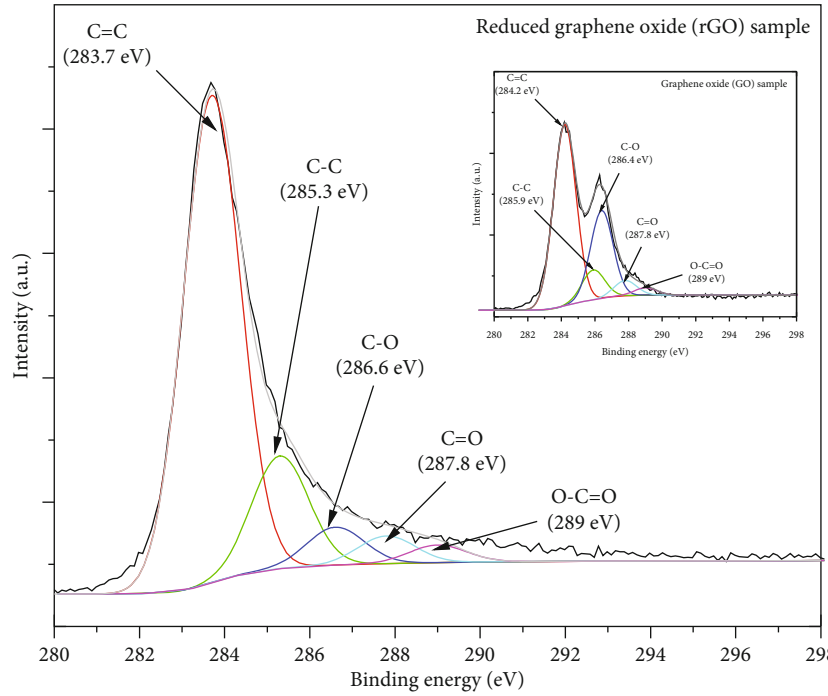

(d)

Figure 2: (a) TEM image of AuNPs. (b) XRD pattern of the AuNPs. (c) Raman spectra of graphite, GO, and rGO. (d) C1s region XPS spectra of rGO and GO (inset).

AuNPs with a more uniform and larger size than AuNPs in sample B. The accumulation of AuNPs at defective sites on rGO sheets in sample B causes the fluctuation in the size. Relying on the analysis from Figure 3, two mechanisms for the combination of AuNPs and rGO sheets are selected to study the effect of AuNPs on gas detecting characteristics of rGO-based sensors in this paper. To investigate the chemical composition and electronic state, the XPS spectra of Au 4f core for the stack (sample A) and composite (sample B) are depicted in Figures 3(e) and 3(f), respectively. Two dominant peaks that ascribed to the binding energies of Au $4f_{7/2}$ and Au $4f_{5/2}$ were clearly shown. Compared with the characteristic peaks of metallic Au° (Au $4f_{7/2} \sim 84.0$ and Au $4f_{5/2} \sim 87.7$ eV), both stack and composite samples show a red-shifted movement in the position of Au $4f_{5/2}$ peaks, e.g., from 84.0 eV to 83.8 eV for the stack and 83.3 eV for composite, respectively. The peak movement results from the electron transfer from the rGO sheet to the AuNPs, indicating that an interaction exists between AuNPs and the rGO framework. Also, the negative shift of the composite is significantly lower (0.7 eV) than that of the stack (0.2 eV). From the above analysis, one can see that the chemical bonding between rGO and AuNPs may predominate in the composite sample while physical bonding prevails in the stack sample.

Figure 4(a) shows the UV-Vis absorption spectra of A, B, and bare rGO samples. A peak at 270 nm, ascribed to the conjugated C-C bonds of the rGO material, is observed in all samples. It indicates that the GO sheets are converted to rGO sheets [11]. Also, the absorption spectrum is a reliable tool for investigating AuNPs in A and B samples. The surface plasmon resonance peak occurs when light passes through nanoparticles, and its position depends on the size and shape of particles [12, 13]. Based on Mie's theory, Huang and El-Sayed and Tri et al. reported that the absorption peak at 520 nm is typical for 20 nm AuNPs, and an increase in particle size causes the red shift of the absorption peak [13–15]. The surface plasmon resonance peak in the stack sample appears at 520 nm, indicating that the as-synthesized AuNP size is around 20 nm. The features of UV-Vis absorption spectra are consistent with the characteristics of AuNPs reported on Cytodiagnostics and NanoComposix websites [16, 17], and in agreement with what we observed from the TEM image. Specifically, the surface plasmon resonance peak of the composite sample is shifted to 610 nm with a stronger intensity in comparison to the stack sample. Cittadini et al. indicate that the red shift of the plasmon absorption is attributed to not only an electron transfer to AuNPs and sp^2-hybridized carbon atoms of rGO but also the stronger coupling of the localized plasmon on neighboring AuNPs [18]. In other words, the interparticle distance decreases and induces the delocalizing of conduction electrons near each particle surface and shares amongst neighboring particles. As inferred from the AFM and SEM images, the red shift of the absorption peak in the composite sample was attributed to the agglomeration of the AuNPs. Figure 4(b) shows the current-voltage characteristics (I-V) of the fabricated devices. The linear and symmetric features in both negative and positive biased indicated the Ohmic contact behavior. The contact feature did not change after hybridized rGO with AuNPs in layer-by-layer (stack) or composite samples. It confirms that the fabrication device is a type of chemiresistor, which operates based on the change of

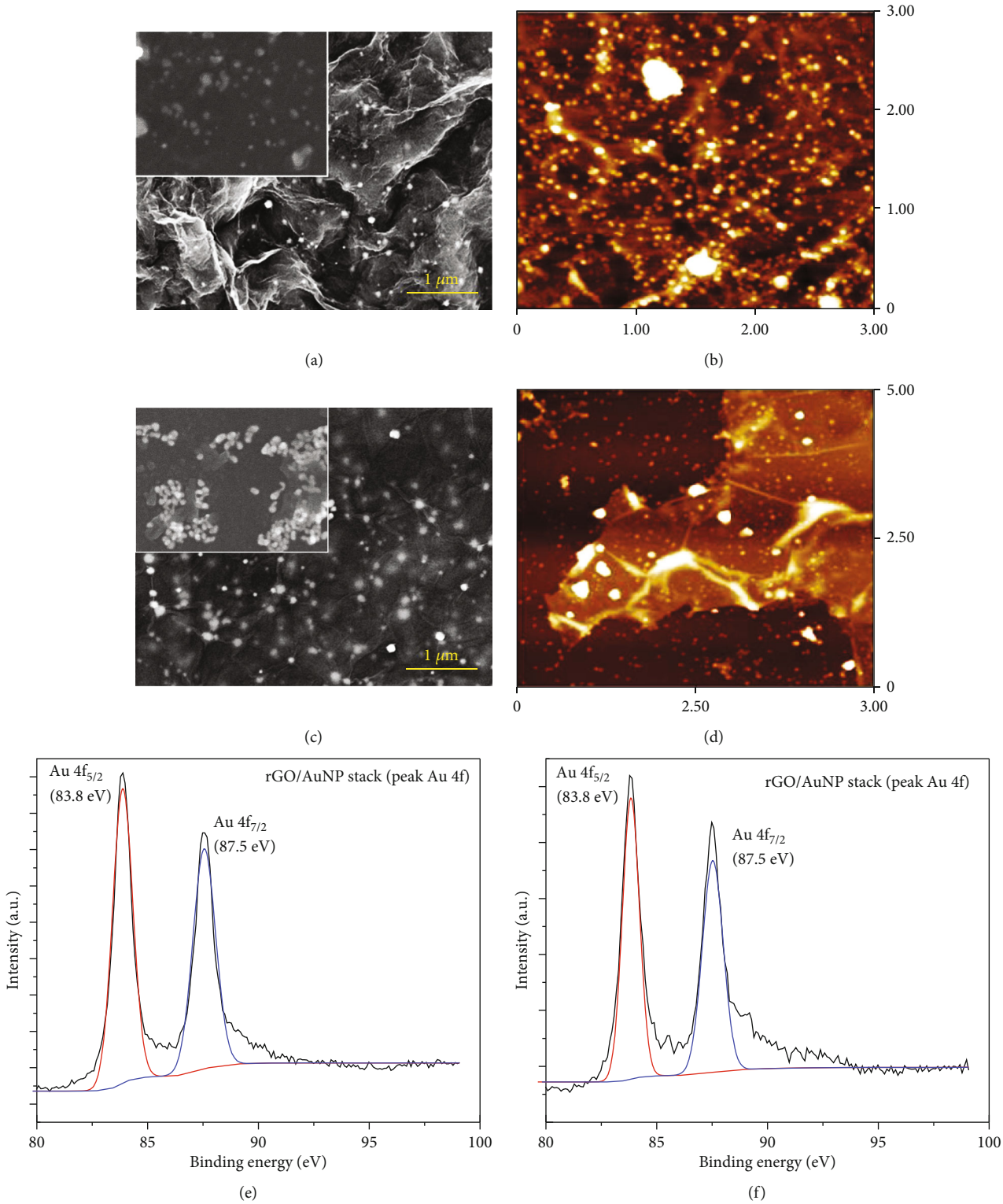

Figure 3: SEM and AFM images of sample A (a, b) and sample B (c, d). XPS spectra of the Au 4f core level region for sample A (e) and sample B (f).

resistance in the presence of an analyte. Thus, the hybridization of AuNPs with rGO is expected to contribute to improving conductivity, leading to a better sensing performance. Indeed, the electrical conductivity of stack and composite samples significantly increase in comparison to rGO after being integrated with AuNPs as shown in Figure 4(b). This result somewhat elucidates the crucial role of AuNPs in enhancing sensing performance.

Figure 5(a) shows the response of the rGO/AuNP stack, rGO-AuNP composite, and bare rGO samples with NH_3

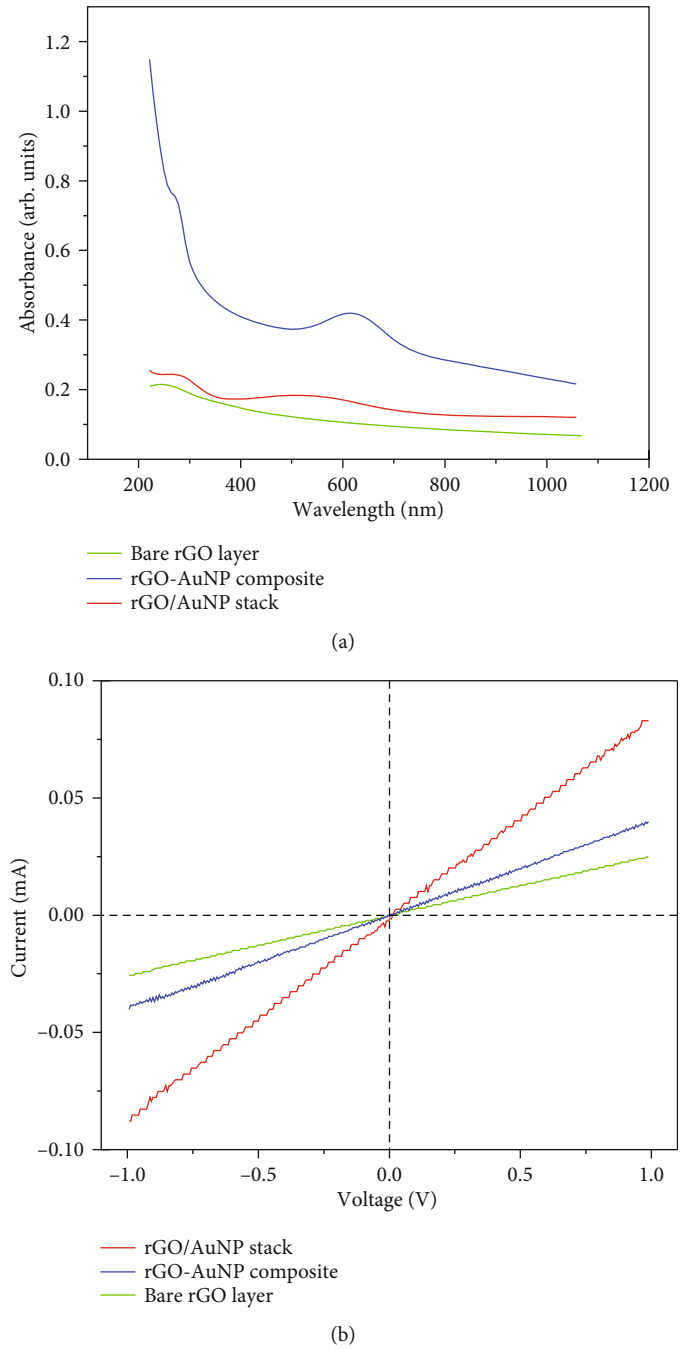

Figure 4: (a) UV-Vis spectra of samples A and B, (b) I-V characteristics of samples A and B, respectively.

gas at room temperature. In general, we observe an increase in their resistances upon the exposure to NH_3 for all fabricated samples. The mechanism of increasing resistance in the presence of NH_3 gas is explained as follows: rGO and hybridized AuNPs with rGO sensing layers have *p*-type characteristics wherein holes act as the majority carriers. The electron donor effect of NH_3 gas molecules (reducing agent) will deplete the hole concentration in sensing layers upon adsorption which leads to an increase in resistance of sensor devices [1, 4, 6, 10], [19, 20]. Our results are comparable to the report of Sivalingam and Balasubramanian who used rGO/Au hybrid nanostructure for detecting 10,000 ppm of NH_3 gas at RT with the highest sensitivity of 10% [5]. Zhang et al. indicated that adding Ag nanoparticles helps to increase sensitivity from 12% (for rGO) to 40% (for Ag-rGO) [21]. The main purpose of this study is to experimentally elucidate the role and effect of the combination way between AuNPs and rGO in improving sensor efficiency through two hybridized structures: composite versus layer-by-layer (stack). Figure 5(a) shows that the response of the bare rGO layer is 9%, but it is considerably enhanced when the AuNPs are incorporated into rGO sheets, e.g., 39% and 53% for the stack and composite samples, respectively. The improvement of NH_3 gas-sensing properties of bare rGO by incorporating

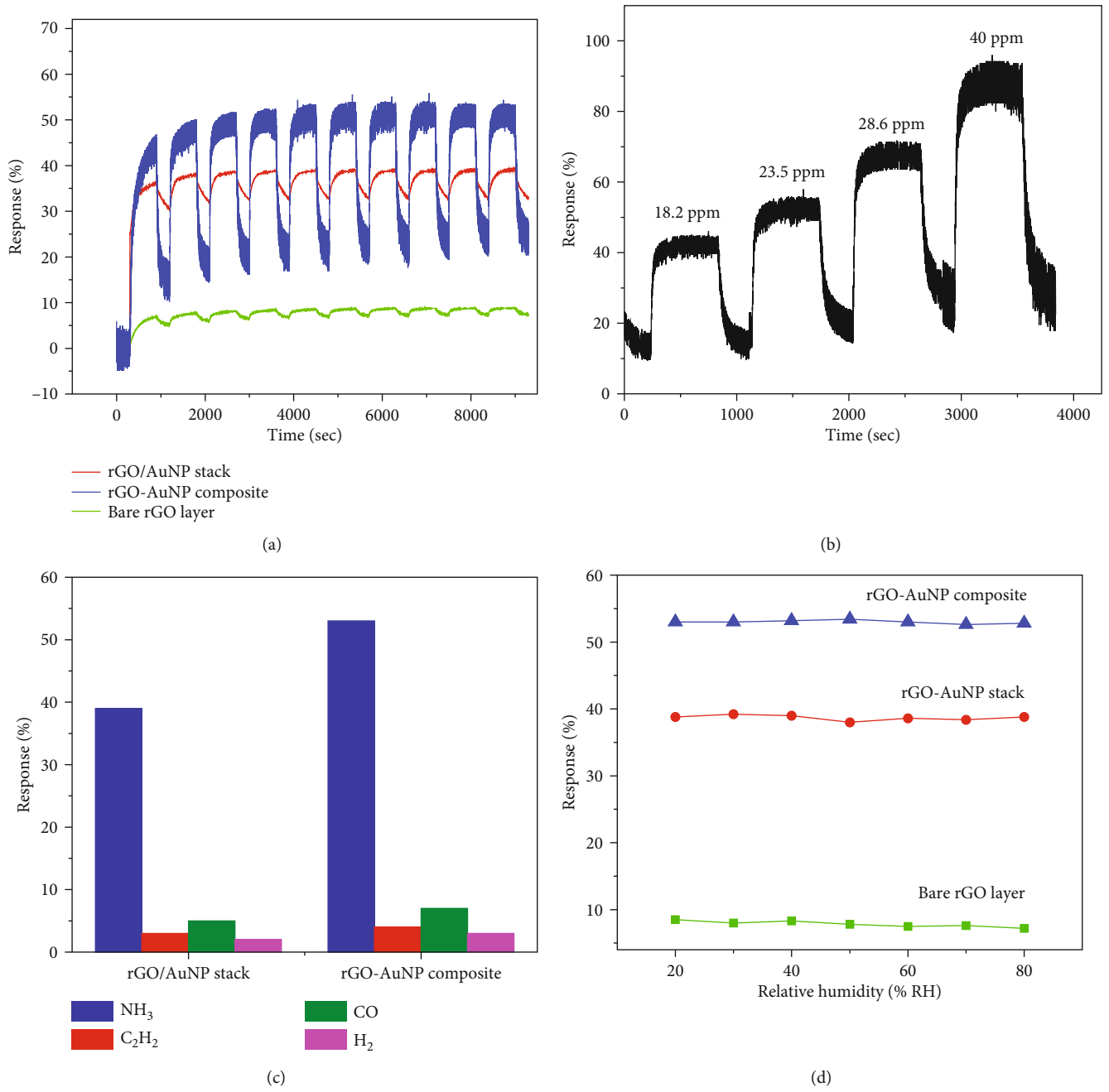

Figure 5: (a) Ten-cycle responses of the bare rGO, stack, and composite samples to 23.5 ppm NH_3 at room temperature with 40% RH, indicating good stability of the sensors. (b) Four-cycle responses of the composite sample to different concentrations of NH_3 ranges from 18 to 40 ppm under room temperature with 40% RH. (c) The selectivity of the stack and composite sensors to NH_3 gas (fixed concentration of 23.5 ppm) and other target gases. (d) The response of the bare rGO, stack, and composite to 23 ppm NH_3 under RH from 20 to 80%.

AuNPs is mainly due to the combined effect of the catalytic activities and the highly conductive nature of AuNPs. Herein, catalytic effect means that adding of AuNPs on the surface of rGO makes it easier for the chemisorption and dissociation of NH_3 gas to occur at the surface. Notably, the response of the composite sample is significantly higher than that of the stack sample. It is due to differences in the way of binding between AuNPs and rGO in these two samples. As indicated in the XPS spectra, the dominant chemical bond in the composite sample promotes the electron transfer from the defect states to the AuNPs. It not only causes an increase in resonant electron density but also creates energetic electrons in a high-energy state. These resonant electrons are so active that they can liberate from the surface of AuNPs and easily react with the oxygen molecules in the atmosphere to create oxygen absorbents (O_2^-) according to the following reaction [6, 10, 11, 19, 21]:

$$O_2(\text{gas}) + e^- \rightarrow O_2^-(\text{ads}) \quad (2)$$

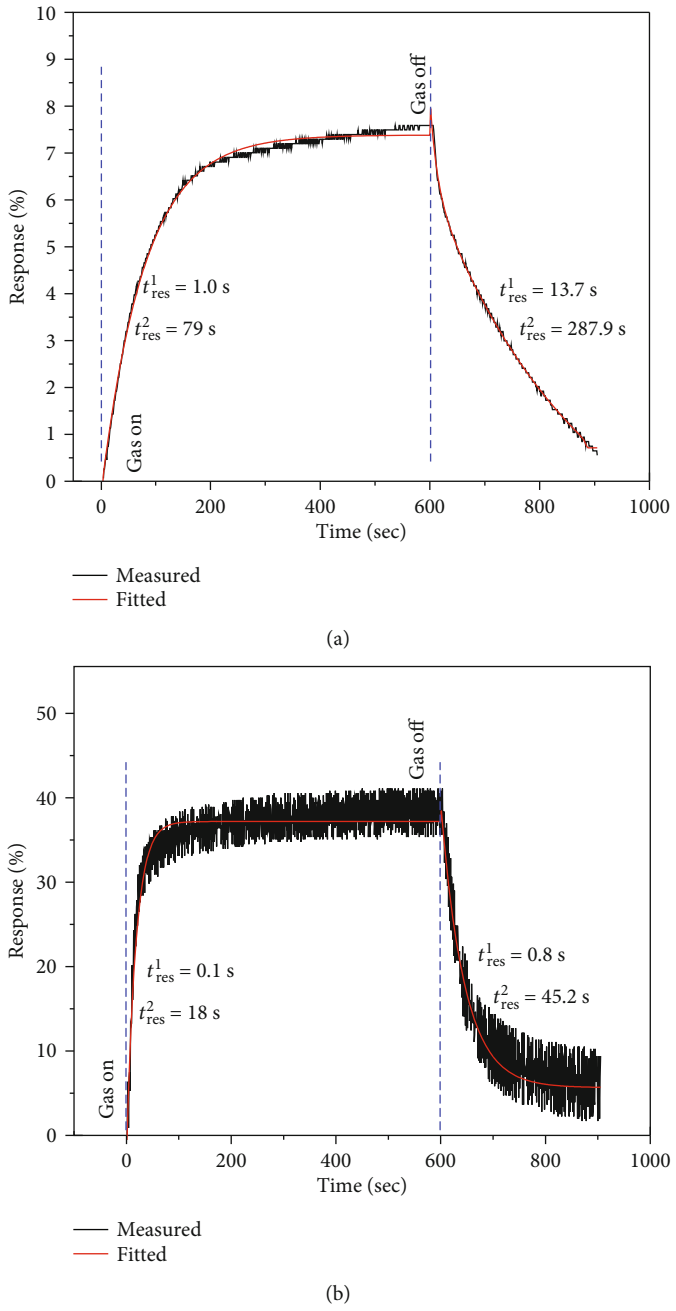

FIGURE 6: Response- and recovery-time analysis of sample A (a), and sample B (b) sensors exposed to 18 ppm of NH_3 gas at room temperature with 40% RH.

When NH_3 gas goes through the test chamber, the NH_3 molecules simultaneously interact with not only sp^3-hybridized carbon atoms of the rGO sheets but also oxygen species adsorbed on the AuNPs [10, 11, 21].

$$4NH_3 + 5O_2^- \rightarrow 4NO + 6H_2O + 5e^- \quad (3)$$

These processes give out electrons back to the rGO sheets, they become less *p*-type, and their resistance increases [10, 11, 22]. By adding this mechanism, composite samples showed a better response than stack samples.

Figure 5(b) shows the response with different NH_3 concentrations at room temperature. The response is found around 45%, 56%, 71%, and 92% for 18 ppm, 23 ppm, 28 ppm, and 40 ppm NH_3 gas, respectively. It confirms the fast speed of sensing activity of sample B and gradually increases as increasing in target gas concentration. Selectivity or the ability to detect different gases is one of the important parameters used to evaluate the performance of a gas sensor. As shown in Figure 5(c), the fabricated sensors exhibit good selectivity for NH_3. The response of the rGO-AuNP composite gas sensor to 23.5 ppm of NH_3 is 5 times more than the response to other target gases, including C_2H_2, CO, and H_2.

From Figure 5(d), we observe that the responses of fabricated sensors to NH_3 are independent of RH value, in the range 20-80%; the response depends solely on the NH_3 concentration. These results verify that the rGO-AuNP composite-based gas sensor is highly selective and can be considered as a potential sensing material for the detection of NH_3. The next parameter of interest is the response time. Figure 6 reveals the experimental and fitted response curves of the stack (a) and composite (b) samples in one cycle of NH_3 gas flow. The response and recovery times are fitted via biexponential function equations [20, 23, 24]:

$$R_g = R_a + A_1\left(1 - e^{-t/t^1_{res}}\right) + A_2\left(1 - e^{-t/t^2_{res}}\right),$$
$$R_g = R_a + A_3.e^{-t/t^1_{rec}} + A_4.e^{-t/t^2_{rec}}, \quad (4)$$

where A_1, A_2, A_3, and A_4 are positive constants; t^1_{res} and t^2_{res} illustrate fast and slow response times while t^1_{rec} and t^2_{rec} indicate fast and slow recovery times. There is a significant match between the experiment and theory analyses. Inferred from the fitted data in Figure 6(b), the composite structure shows the excellent time constants as follows: the response times are $t^1_{res} = 0.1$ s and $t^2_{res} = 18$ s; the recovery times are $t^1_{rec} = 0.8$ s and $t^2_{rec} = 45.2$ s. For comparison, the time constants of the stack are much longer $t^1_{res} = 1.0$ s, $t^2_{res} = 79$ s, $t^1_{rec} = 13.7$ s, and $t^2_{rec} = 287.9$ s as shown in Figure 6(a). According to reports of Osorio-Arrieta et al. and D'Arsié et al., the t^1 and t^2 values in sensors may be related to different interactions of the NH_3 molecules with the sensing layer. The fast phenomena (the short time t^1) can arise in adsorption of gas molecules onto the sensing film surface; meantime, the quite slow phenomena (the long time t^2) can be originated from a diffusion of NH_3 molecules into the sensing film [17, 20]. Also, the interaction of the NH_3 molecules with adsorbed oxygen species is weaker than the interaction of the NH_3 molecules with sp^3-hybridized carbon atoms. Thus, the interaction between NH_3 molecules and the adsorbed oxygen species may be responsible for faster response/recovery process; meanwhile, the NH_3 molecules directly interact with sp^3-hybridized carbon atoms causing slower response/recovery performance [4, 11]. These aforementioned results indicate that the reaction between NH_3 and oxygen absorbents plays a dominant role in the sensor mechanism of composite samples, while the reaction between NH_3 and sp^3-hybridized atoms is in the majority in sensor mechanism of stack samples.

4. Conclusions

By changing the combination of rGO and AuNPs in this study, we have clarified the role and effect of AuNPs in improving NH_3-sensing performance as follows: first, the fundamental mechanism of a chemiresistor sensor solely depends on the resistance change; thus, adding AuNPs dramatically improves the electrical conductivity of rGO, leading to a better electron transfer to the electrodes via rGO; second, it is involved in the catalytic effect of AuNPs, which makes it favorable for the chemisorption and dissociation of NH_3 gas at the surface; the last and also the significant finding in this study is that the difference of the NH_3 gas sensor mechanism depends on how the AuNPs and the rGO link, whether it is chemical or physical bonding. If the physical bond as seen in the stack sample was formed, the main mechanism of the gas sensor is the reaction between NH_3 and sp^3-hybridized carbon atoms. In the case of chemical bonds, as found in composite samples, NH_3 not only reacts with sp^3-hybridized atoms but also reacts primarily with oxygen absorbents on the surface of AuNPs caused by resonant electrons. For these reasons, when hybridization of AuNPs with rGO by chemical bonding is formed, this combination possesses a better NH_3-sensing performance compared to other counterparts.

Data Availability

The data used to support the findings of this study are available from the corresponding author upon request.

Conflicts of Interest

The authors declare that there is no conflict of interest regarding the publication of this article.

Acknowledgments

This research was funded by the Vietnam National Foundation for Science and Technology Development (NAFOSTED) under grant number 103.02-2018.352.

References

[1] S. Basu and S. Hazra, "Graphene–noble metal nanocomposites and applications for hydrogen sensors," *C*, vol. 3, no. 4, 2017.

[2] U. Latif and F. L. Dickert, "Graphene hybrid materials in gas sensing applications," *Sensors*, vol. 15, no. 12, pp. 30504–30524, 2015.

[3] D. T. Phan and G. S. Chung, "A novel Pd nanocube-graphene hybrid for hydrogen detection," *Sensors and Actuators B: Chemical*, vol. 199, pp. 354–360, 2014.

[4] H. Zhang, Q. Li, J. Huang, Y. du, and S. C. Ruan, "Reduced graphene oxide/Au nanocomposite for NO_2 sensing at low operating temperature," *Sensors*, vol. 16, no. 7, 2016.

[5] M. M. Sivalingam and K. Balasubramanian, "Influence of the concentration of reducing agent on gold nanoparticles decorated reduced graphene oxide and its ammonia sensing performance," *Applied Physics A: Materials Science & Processing*, vol. 123, no. 4, 2017.

[6] M. S. Choi, A. Mirzaei, J. H. Bang, W. Oum, S. S. Kim, and H. W. Kim, "Improvement of NO2 sensing properties in Pd functionalized reduced graphene oxides by electron-beam irradiation," *Frontiers in Materials*, vol. 6, 2019.

[7] H. Wang, Q. Feng, Y. Cheng et al., "Atomic bonding between metal and graphene," *Journal of Physical Chemistry C*, vol. 117, no. 9, pp. 4632–4638, 2013.

[8] R. Zan, U. Bangert, Q. Ramasse, and K. S. Novoselov, "Interaction of metals with suspended graphene observed by transmission electron microscopy," *Journal of Physical Chemistry Letters*, vol. 3, no. 7, pp. 953–958, 2012.

[9] P. A. Khomyakov, G. Giovannetti, P. C. Rusu, G. Brocks, J. Van Den Brink, and P. J. Kelly, "First-principles study of the interaction and charge transfer between graphene and metals," *Physical Review B*, vol. 79, no. 19, pp. 1–12, 2009.

[10] M. Gautam and A. H. Jayatissa, "Ammonia gas sensing behavior of graphene surface decorated with gold nanoparticles," *Solid-State Electronics*, vol. 78, pp. 159–165, 2012.

[11] Q. T. Tran, H. T. M. Hoa, D.-H. Yoo et al., "Reduced graphene oxide as an over-coating layer on silver nanostructures for detecting NH_3 gas at room temperature," *Sensors and Actuators B: Chemical*, vol. 194, pp. 45–50, 2014.

[12] G. Goncalves, P. A. A. P. Marques, C. M. Granadeiro, H. I. S. Nogueira, M. K. Singh, and J. Grácio, "Surface modification of graphene nanosheets with gold nanoparticles : the role of oxygen moieties at graphene surface on gold nucleation and growth," *Chemistry of Materials*, vol. 21, no. 20, pp. 4796–4802, 2009.

[13] N. T. Khoa, S. W. Kim, D. Yoo, E. J. Kim, and S. H. Hahn, "Size-dependent work function and catalytic performance of gold nanoparticles decorated graphene oxide sheets," *Applied Catalysis A: General*, vol. 469, pp. 159–164, 2014.

[14] X. Huang and M. A. El-Sayed, "Gold nanoparticles: optical properties and implementations in cancer diagnosis and photothermal therapy," *Journal of Advanced Research*, vol. 1, no. 1, pp. 13–28, 2010.

[15] J. C. Martínez, N. A. Chequer, J. L. González, and T. Cordova, "Alternative metodology for gold nanoparticles diameter characterization using PCA technique and UV-VIS spectrophotometry," *Nanoscience and Nanotechnology*, vol. 2, no. 6, pp. 184–189, 2012.

[16] Ronson, *Uv/Vis/Ir spectroscopy analysis of nanoparticles*, vol. 1, Nano Composix, 2012.

[17] L. D'Arsié, V. Alijani, S. T. S. Brunelli et al., "Improved recovery time and sensitivity to H_2 and NH_3 at room temperature with SnOx vertical nanopillars on ITO," *Scientific Reports*, vol. 8, no. 1, pp. 10028-10029, 2018.

[18] M. Cittadini, M. Bersani, F. Perrozzi, L. Ottaviano, W. Wlodarski, and A. Martucci, "Graphene oxide coupled with gold nanoparticles for localized surface plasmon resonance based gas sensor," *Carbon*, vol. 69, pp. 452–459, 2014.

[19] S. Gupta Chatterjee, S. Chatterjee, A. K. Ray, and A. K. Chakraborty, "Graphene–metal oxide nanohybrids for toxic gas sensor: A review," *Sensors and Actuators B: Chemical*, vol. 221, pp. 1170–1181, 2015.

[20] D. L. Osorio-Arrieta, J. L. Muñoz-Mata, G. Beltrán-Pérez et al., "Reduction of the measurement time by the prediction of the steady-state response for quartz crystal microbalance gas sensors," *Sensors*, vol. 18, no. 8, 2018.

[21] L. Zhang, Q. Tan, H. Kou, D. Wu, W. Zhang, and J. Xiong, "Highly sensitive NH_3 wireless sensor based on Ag-RGO composite operated at room-temperature," *Scientific Reports*, vol. 9, no. 1, article 9942, 2019.

[22] M. Yang, Y. Wang, L. Dong et al., "Gas sensors based on chemically reduced holey graphene oxide thin films," *Nanoscale Research Letters*, vol. 14, no. 1, pp. 218–228, 2019.

[23] V. Postica and L. Oleg, "Synthesis of ag-doped ZnO nanostructured films for UV photodetectors," in *Proceeding of the 6th International Conference Telecommunications, Electronics and Informatics*, pp. 488–491, 2018.

[24] D. Gedamu, I. Paulowicz, S. Kaps et al., "Rapid fabrication technique for interpenetrated ZnO nanotetrapod networks for fast UV sensors," *Advanced Materials*, vol. 26, no. 10, pp. 1541–1550, 2014.